

Leading-edge Vortices Control on a Delta Wing by Micromachined Sensors and Actuators

Gwo-Bin Lee,* Yu-Chong Tai,# Fukang Jiang,# Charles Grosjean,# Chang Liu**,
and Chih-Ming Ho[†]

*National Cheng-Kung University, Tainan, Taiwan, Republic of China

#California Institute of Technology, Pasadena, CA, USA

**University of Illinois at Urbana-Champaign, Urbana, IL, USA

[†]University of California, Los Angeles, CA, USA

Abstract

Instead of using conventional flaps to generate torques, we explore the feasibility of applying micromachined sensors and actuators to control leading-edge vortices, and consequently, provide sufficient moments for flight control. By utilizing a “flexible skin” containing 64 micromachined shear stress sensors, instantaneous separation line on the leading edges can be detected. We applied micro-actuators to manipulate the flow inside the boundary layer around the separation region, resulting in a large change in the three-axis moments. Surface pressure measurements and flow visualization on the upper side of the delta wing have been conducted to explore the physical mechanisms of torque generation and show how micro-actuators alter the vortex structure.

Introduction

Micromachining technology for fabrication of miniature sensors and actuators on the order of microns became available in the 1980's. MEMS (Micro -Electro-Mechanical-Systems) consisting of a large number of micro-sensors, micro-actuators and logic electronics can be manufactured with this technology. MEMS allow us to fabricate micro-sensors and micro-actuators that match the length scales of the investigated phenomena in the scale of microns. Since micromachining is compatible with IC processes, we can integrate these miniature transducers with microelectronics to complete the loop of sensing, information processing, and actuation on a single chip. It will enable us to perform real-time control of time-varying events common in different fields of research.

The basic MEMS fabrication techniques include (1) *bulk micromachining*, (2) *surface micromachining*, and (3) *LIGA* (Lithographie Galvanoformung, and Abformung; German acronym for x-ray lithography, electroplating, and electromolding). The detailed information about MEMS fabrication techniques can be found in the literature.¹⁻² MEMS-based transducers have been used on flow control.³ We applied the MEMS-based transducers to control flow on a wing,⁴ flow in the turbulent boundary layer,⁵⁻⁶ and flow in micron-size channels.⁷

Many efforts on the control of vortical flow over delta wings have been reported in the literature. These approaches can be classified as *blowing*,⁸⁻⁹ *suction*,¹⁰ *mechanical flaps*,¹¹⁻¹² and *heating*.¹³ Bradley and Wray⁸ showed that vortex breakdown could be delayed to higher angles of attack by blowing a stream of high-pressure air parallel to the leading edges. The blowing momentum coefficient, defined as $C_{\mu} = \dot{m} V_j / q_{\infty} S$, equals 0.088, where \dot{m} , V_j , q_{∞} , and S are mass flow rate, injection velocity, dynamic pressure, and wing area, respectively. As a result, higher lift can be achieved. Wood and Roberts⁹ conducted an experiment using tangential mass injection to control leading edge vortices. Their results showed that about a 30 % increase of the normal force coefficient can be obtained and significant rolling moments can be produced at high angles of attack. The pressure data presented by Wood and Roberts suggested that the vortex structure had been strengthened and localized at high angles of attack by blowing. Thus, larger lift can be generated.

Similarly, suction has been used on the leeward side of delta wings to investigate the possibility of controlling leading edge vortices. Hummel¹⁰ employed suction to the vortex cores downstream of the wing's trailing

edge and investigated the effect of suction on the lift. He found that an increase of lift at high angles of attack could be achieved.

Large flaps with various geometries have been employed at different locations to explore the effects on leading edge vortices. Marchman¹¹ employed the upward deflected flap at the leading edges to investigate the effect of these devices on the lift and drag. His data showed that lift increases at low angles of attack. However, the loss of maximum lift was also observed. He suggested that swirl angle be increased by employing deflected flaps. Hence, a lower peak lift occurs due to the earlier vortex breakdown. His data indicated that a flap is an effective way to control leading edge vortices at low angles of attack. Later, Wahls, Vess, and Moskovitz¹² conducted experiments using vertically deployed “apex fences” on a delta wing to improve the lift force and generate a pitching moment. The flow visualization showed that fence-generated vortices would interwind with the original vortex which is separated from the leading edges and produce a higher suction level. This higher suction level between the fences indicates that a nose-up pitching moment can be obtained.

Heating of the surface is not very effective when compared to other methods. Marchman¹³ investigated the effects of heating on the leading edge vortices. He found that lift and pitching moment did not change significantly while heating the surface to twice the free-stream temperature.

These methods either alter the vorticity generation near the leading edges or change the vorticity convection along the vortex core. However for a delta wing with rounded leading edges, flow could separate at different locations depending on local curvature, Reynolds number, and pressure gradient. Therefore, the separation line along the leading edges could be a curve line, especially under dynamic maneuvering. In order to control this curve line efficiently, we propose to use distributed micro-actuators. Using micro-actuators to control delta wings has advantages over traditional control surfaces. Frequency responses could be faster and spatial resolution could be improved due to the small inertia of micro-actuators. Since the size of these micro-actuators could be very small, they have small radar observability when compared with conventional control surfaces. Micromachined sensors and actuators can be batch-fabricated by using photolithography techniques such that unit transducer cost can be greatly reduced. Most importantly, micromachining technology is compatible with IC processes. It is possible to

integrate micro-actuators, micro-sensors, and microelectronics on the same chip to form a “smart skin” such that active and distributed control can be accomplished.

The surface shear stress distribution can be used to indicate flow separation which is the physical mechanism used for flow control. A micromachined shear stress sensor has been fabricated and proven high sensitivity for air operation¹⁴. These sensors will be employed on the leading edges of a delta wing to map out shear stress distribution and detect instantaneous separation lines. After a separation line has been detected by these shear stress sensors, we used micro-actuators to control leading-edge vortices.

We will use micro-actuators to manipulate the thin boundary layer near the leading edges of a delta wing, thereby altering the flow separation location and vortex structure. Each leading-edge vortex¹⁵⁻¹⁶ contributes a large portion of lift to the delta wings. At high angles of attack, the lift force generated by these two leading edge vortices can be as high as 40 % for slender delta wings¹⁷. Therefore, if we can break the symmetry of these vortices, we will be able to generate a rolling moment, or even pitching and yawing moments by appropriate spatial actuation.

If the size of the micro-actuators is comparable to the boundary layer thickness on the leading edges of a delta wing, it is possible to perturb the flow and break the symmetry of the primary vortices by activating micro-actuators at proper locations.¹⁸⁻¹⁹ A micro-actuator is required to deflect 1 - 2 mm out-of-plane (or match the boundary layer thickness) and withstand large aerodynamic loading on the order of several hundred μN . A permalloy flap magnetic actuator and a balloon actuator have been developed to satisfy the requirements and used for aerodynamic testing in wind tunnel facility.²⁰⁻²¹ Surface pressure measurements and flow visualization, have been conducted to examine the physical mechanisms for torque generation.

SEPARATION LINE DETECTION

A micromachined shear-stress sensor has been fabricated to measure the separation point along the leading edges of a delta wing. It is a thermal shear-stress sensor that relates the convective heat transfer to surface shear stress. The size of the sensor is $250\ \mu\text{m} \times 250\ \mu\text{m}$. The shear-stress sensor consists of a polysilicon resistor, $2\ \mu\text{m} \times 80\ \mu\text{m}$, located on a thin silicon-nitride diaphragm, which is located on top of a vacuum cavity (Fig. 1). The vacuum cavity prevents heat transfer to the substrate and increases the sensitivity by at least one order of magnitude over their traditional counterparts.¹⁷

Figure 2 shows a shear-stress sensor mounted on a rod fitted in the leading edge of a delta wing. By rotating the rod, one can obtain the wall shear stress at different locations around the leading edge when a single sensor is used. We intend to detect an effective control location in the three dimensional flow by using micromachined shear stress sensors. This location should be close to the separation point. However, it is non-trivial to define a separation position in this 3-D flow.²² In this work, an operational definition was used to determine the location where the actuation is most effective. Typically, the RMS (Root-Mean-Square) value of the surface shear stress stays low on the pressure side of the wing and increases towards the suction side of the wing. A sharp increase in the RMS shear stress is observed at a certain location (Fig. 3). It is reasonable to use the sharp increase as an indication of a change in the state of flow. This sharp demarcation may not be the exact 3-D separation location following the strict definition, but we believe the location of the sudden increase of RMS shear stress is at least very close to the separation location. By placing the sensor at various locations on the leading edges, one can map out the surface shear stress along the leading edge from the apex to the trailing edge (Fig. 4). A curved demarcation line is determined from the sharp rise in the surface shear stress and thus represents the “separation line”.

The “separation line” is observed to be a curved line. This means that the separation is indeed three dimensional in nature. Furthermore, the separation zone is found to change with velocity. For higher velocities, the location of the separation line moves toward the pressure surface (lower surface). During maneuvering conditions, large variations in the separation zone location may occur. Therefore, real-time sensing and distributed actuation are necessary to determine the instantaneous separation locations. These separation locations are essential for achieving optimum control.

The successful detection of the “separation line” has been achieved by using a single sensor located on the leading edge rod. However, the *instantaneous* “separation line” cannot be detected by this setup. During dynamic maneuvering, we expect that the separation line will change with local flow conditions. Devices that can wrap around the curved surface with enough sensing elements to detect this instantaneous “separation line” are necessary for this task.

In order to effectively detect the instantaneous “separation line”, a flexible skin sensor with shear stress sensor arrays has been designed and fabricated for this study.²³ Figure 5 shows a picture of the 1 cm x 3.2 cm skin which has a thickness of 75 μm . This skin has two columns of 32 shear stress sensors and can cover the 1-cm wide portion of the leading edge completely. It consists of hundreds of small silicon islands connected by two layers of high strength polyimide. Excellent flexibility has been achieved such that we can easily wrap this skin on a curved surface.

The flexible skin sensor was attached to a circular cylinder to prove that it is capable of detecting separation (Fig. 6). The separation position for flow over a circular cylinder was well documented in the literature.²⁴ For Reynolds numbers less than 2×10^5 , the flow over a circular cylinder is laminar. The corresponding position for the separation point is at about 80° as measured from the stagnation point. Bellhouse²⁵ used a single hot-film sensor to detect the separation point and reported that the DC signal reaches a local minimum at the separation point, and a sudden jump in the RMS signal occurs after flow separates. Our measurements showed exactly the same trend. Figure 7 indicates that the separation point is indeed located near 80° , where a minimum value of DC output takes place. An abrupt increase in the fluctuation of signal was also observed in Fig. 8.

After testing the flexible skin with shear stress arrays on a circular cylinder, the flexible skin sensor was placed on the leading edge of a delta wing to detect the instantaneous separation line. Figure 9 shows the results obtained by the flexible skin sensor at $\text{AOA}=30^\circ$, $L=28$ cm (where L is the distance measured from the apex) compared with a single sensor output. Very good agreement has been observed as shown in this figure. In order to detect the separation line along the leading edges, the flexible skin sensor was attached to a small piece of a 2 cm-

long circular cylinder and moved from the apex to the trailing edge. The information regarding separation line will be used to correlate micro-actuator locations for optimum flow control.

TORQUE GENERATION BY USING MICRO-ACTUATORS

Two different kinds of micro actuators have been used for wind tunnel testing. The first one is a magnetic micro-actuator with out-of-plane deflection lengths of 1 and 2 mm (Fig. 10).²⁰ It is a surface-micromachined flap activated by an external magnetic field. A silicon nitride plate/beam structure is deposited on the top of a 3 μm -thick phosphosilicate glass (PSG) sacrificial layer. Then a 5 μm -thick permalloy ($\text{Ni}_{80}\text{Fe}_{20}$) layer is electroplated on the plate as a magnetic inductive material. After electroplating, the PSG is removed by HF wet etching, and a unique rinse/drying process is used to avoid adhesion problems. In order to increase the strength of the micro-actuators, a torsional bar has been integrated at the end of support beams.

Another pneumatically-driven silicone rubber membrane (balloon actuator) has been designed and fabricated for this work.²¹ Starting with a <100> silicon wafer, back-side cavities are etched anisotropically using KOH, forming a square free-standing membrane. A thin layer of Parylene C is deposited on the front side as a sacrificial layer. Then silicone rubber is spin-coated on the front side. The size of each balloon is 2.3x 8.6 mm. The vertical deflection length for the balloon actuators is about 2 mm at gauge pressure of 6 psi (Fig. 11). During the testing, we found some portions of micro flap actuators had been broken due to higher wind loading. Conversely, micro balloon actuators were found to be much more robust. No damage to these micro-actuators was observed during the wind tunnel testing. In addition to wind tunnel testing, several strips of balloon actuators were attached to a small test section of F-15 fighter jet wing for flight test.²¹ The maximum Mach number tested was 0.9 Mach number and temperatures ranged from -9 $^{\circ}\text{F}$ to 110 $^{\circ}\text{F}$. It was found that all the balloon actuators survived the harsh flight test several times, which demonstrates the robustness of the devices.

The delta wing used for wind tunnel testing is a triangular plate with a sweep angle of 56.5° and a chord length of 30.48 cm. The radius at the leading edge is 1.3 cm. This wing was mounted on a six-component force/moment transducer that recorded forces and moments in all three axes. A linear array of micro-actuators was placed at one of the rounded leading edges (Fig. 12). The location of the actuators is indicated by angle θ , which is defined as 0° for lower surface and 180° for upper surface. The torque is measured as a function of θ for angles of attack ranging from 5° to 35° . The results were normalized using the magnitude generated by a single vortex. First, the magnitude of vortex lift (L_v) at a certain angle of attack is calculated from Polhamus's theory.¹⁶ Then, this vortex lift is multiplied by a characteristic length (d), which is the distance from the centerline to the centroid of the half wing, to form a reference torque. The reference torque is used to normalize torque change generated by micro actuators.

Rolling Moment For micro Actuators

We only show results at an angle of attack (AOA) of 25° here since data for the other AOAs have a similar trend.²⁶ Figure 13 shows the results of the induced rolling moment for two types of micro-actuators. The maximum torque occurs at $\theta=50^\circ$ and can be as high as +12 % for 1 mm flap actuators. For large values of θ , the normalized rolling moment becomes negative. The negative torque can be as large as -14 % at $\theta=80^\circ$ for 1 mm flap actuators. The data for balloon actuators also show the same trend. However, the amplitude of the induced rolling moment is smaller for balloon actuator.

The adverse pressure gradient generated by balloon actuators is smaller than that generated by flap actuators. Thus, it could be one of the reasons for smaller torque generation. The other cause for smaller torque generation is surface contour of the actuators. Direction of separation shear layer is directly related to surface contour. For balloon actuators, the shear layer is closer to wing surface due to curved surface contour. Conversely, the shear layer for flap actuators is pushed away from surface since flow separates at the edge of a sharp surface. As a result, the vortex structure for these two cases could be very different. Flow visualization shows that vortex has been pushed away further for micro-flap actuators, resulting in a larger rolling moment.

We anticipate that vortex structure could be very sensitive to deflection angle of micro-actuators since flow tends to separate near the edge of a sharp surface. Miniature mechanical actuators with various deflection angles (β) have been installed at $\theta=50^\circ$ on the rounded leading edge of a delta wing at $AOA=25^\circ$ to investigate aerodynamic performance (Fig. 14). Preliminary results are shown in Figure 15. For different Reynolds numbers, the result always favors the cases with smaller deflection angles. For example, the change in the normalized rolling moment is 32 % for $\beta=30^\circ$, which is almost two times larger than the case with $\beta=160^\circ$ (17%). For smaller deflection angles, the separation shear layer has been moved away from wing surface, resulting in a larger moment arm, thus, a larger rolling moment can be induced.

We also used mechanical actuators for some wind tunnel testing. The mechanical actuator is made of 1/1000th-inch-thick stainless shim stock and has the same deflection length as micro actuators except that the stiffness of the mechanical actuator is larger. Figure 16 represents the schematic of a mechanical actuator. A long Stripe-type mechanical actuator is attached on the inner rod, which can be rotated by a servomotor. By rotating this inner rod, mechanical actuators can be extended 1 or 2 mm out of plane through a small slot on the leading edges. Data for 2 mm actuators are shown in Fig. 17. We found that a rolling moment as large as +35 % can be generated at $\theta=50^\circ$. Similarly, we also found that we can get a very large negative rolling moment at $\theta=80^\circ$.

Two-Sided Actuation Effect

The negative rolling moment at $\theta=80^\circ$ can be employed to obtain an additional rolling moment if another array of actuators is mounted at the proper position on the opposite leading edge. One can generate an additional rolling moment if one activates the actuators on two sides of the leading edges simultaneously. For example, for a wing at $AOA=25^\circ$ (Fig. 17), actuators are mounted at $\theta=50^\circ$ location on one leading edge and at $\theta=80^\circ$ location on the other leading edge. Figure 18 represents the results of the actuation along both leading edges. At $AOA=25^\circ$, the normalized torque at large θ can be as much as - 35%. If the actuators are placed both at $\theta=50^\circ$ along one leading edge and at $\theta=80^\circ$ along the other leading edge, the maximum induced torque reaches a staggering level of

70 %. Moreover, as shown in Fig. 18, the summation of the individual incremental torque is equal to the value obtained by the simultaneous actuation along both leading edges. This indicates that modifications of the vortices on both sides of a delta wing by the actuators seem to act independently.

Maximum Pitching, Yawing, and Rolling Moment Coefficients at different AOA

Extensive investigations for AOA ranging from 5° to 35° have been conducted. Here, we only present the results for 2 mm micro balloon actuators. The data were converted into moment coefficients as shown in Figs. 19-21.

The pitching, yawing and rolling moment coefficients, C_p , C_y , C_r , respectively, are defined in the following:

$$C_p = \frac{\Delta M_p}{QS\bar{c}} \quad (1)$$

$$C_y = \frac{\Delta M_y}{Q Sb} \quad (2)$$

$$C_r = \frac{\Delta M_r}{Q Sb} \quad (3)$$

where ΔM_p , ΔM_y , ΔM_r are changes in the pitching, yawing, and rolling moments induced by micro actuators. Q , S , b , \bar{c} are dynamic pressure, wing area, trailing edge length, and distance from the apex to centroid of the wing, respectively. It was found that one could achieve pitching and rolling moment coefficients of 0.03 and 0.012, respectively. These two values are large enough for most of flight control²⁷. However, the maximum value of the yawing moment coefficient is only 0.0065.

A shorter array of actuators which only covers half of the length from the apex to the trailing edge, called H-A-T (Half-Apex-Trailing edge) actuator, has been used to explore the possibility of increasing control capability. Two actuators which extend simultaneously on both sides of the leading edges have also been tested to increase the induced torques. When we use H-A-T actuators installed on one of the leading edges, it breaks the symmetry of the vortices such that rolling, pitching and yawing moments can be produced. For a more effective way to generate the pitching and the yawing moments, we suggested two possible arrangements of the actuators (Fig. 22). The extensive investigations have been done and detailed results will be discussed in another paper.

Surface Pressure Measurements

Surface pressure measurements conducted by Fink and Taylor²⁵ showed that locations of the maximum suction are directly beneath the vortex cores. This results that one could identify core locations from surface pressure measurements. In this section, the effects of micro actuators on the distribution of the surface pressure on the suction side of the delta wing will be investigated. The goal of these pressure measurements is to explore the interaction between the micro actuators and primary vortices.

A delta wing model with pressure taps on the surface has been designed and fabricated for the purpose of surface pressure measurements. Figure 23 shows a schematic representation of the wing model. In the chordwise direction, seven sections are distributed from $x/c=0.3$ to $x/c=0.9$. At each section, there are 18 measurement points along the half span, including 3 points on the surface of the rounded leading edge.

A commercial solid-state gauge pressure sensor (NPC-1210, Lucas NovaSensor) has been used for this work. The full-scale range of this sensor is 5 psi. By using a constant-current circuit , the sensitivity of the sensor has been calibrated as 0.8 volts/ psi. over the experimental operating range.

A linear array of 2 mm micro-actuators has been installed on one leading edge of a delta wing to investigate the effect of micro-actuators on the aerodynamics of a delta wing. From data in the previous sections, it was found that a large positive rolling moment could be generated at $\theta=50^\circ$, and a large negative rolling moment could be generated at $\theta=80^\circ$. These two positions were then chosen to investigate the effects of micro-actuators on the surface pressure distribution. Figure 24 shows the pressure distribution at 40 % chord location at $AOA= 25^\circ$. Experiments showed that the activation of 2 mm actuators at $\theta=50^\circ$ moves the surface pressure peak outboard, generating a positive rolling moment. Examination of the region close to the leading edge where the micro-actuators start to interact with flow separation, shows a large increase in the pressure distribution occurring near the leading edge. This interaction produces an increase in the normal force, and consequently, generates a positive rolling

moment. On the other hand, experimental results show that the activation of 2 mm actuators at $\theta=80^\circ$ moves the peak of surface pressure inboard, and decreases the suction near the leading edge. As a result, a negative rolling moment is generated (Fig. 25).

Data for each section showed the same trend. Pressure distributions at every cross section for these two cases are shown in Figs. 26-27. It was observed that micro-actuators cause the deformation of the vortex structure. The integration of the pressure distribution along the spanwise direction was used to obtain the rolling moment before and after actuation. Then the change in the rolling moment could be determined accordingly. From the current results, a +37 % change in the normalized rolling moment can be obtained for the case of $\theta=50^\circ$, and a -32 % change in the normalized rolling moment for the $\theta=80^\circ$ case. Results from the integration of the pressure measurements are consistent with those from the six-component sensor, which are +35 % and -35 %, respectively.

Flow Visualization

Data from the surface pressure measurements only reveal the information on the surface of the delta wings. In order to investigate the interaction between the micro-actuators and the vortices, information about the flowfield is necessary to obtain physical insight. Flow visualization of the vortices was chosen for this purpose. In this section, we will use this technique to visualize the flow on the upper side of the delta wing. We will focus on the vortex structure, especially the location of vortex core, to investigate the interaction between the micro-actuators and vortices.

A laser sheet was used to visualize the structure of the vortices, and especially the location of vortex cores. Figure 28 shows the experimental setup for the flow visualization on the upper side of the wing model. To visualize the flow, a sheet of laser light from a pulsed Nd:YAG laser was projected across the wind tunnel and adjusted so as to intercept the delta wing at any chosen chordwise location. Thus, the cross-flow plane can be illuminated to investigate the structure of the vortices. A system consisting of a high-resolution CCD camera, image interface card and IBM PC were used for image acquisition. The tests were conducted in the 1x1-ft² low-speed wind tunnel. This is

a suction-type wind tunnel especially designed for the purpose of flow visualization. The maximum speed of the tunnel is about 18 m/s.

A scaled wing model of the one used in 3x3-ft² wind tunnel was used for flow visualization. Two positions, $\theta=50^\circ$, and 80° were chosen for micro actuation to visualize the effects of micro-actuators on the vortex structure. Instead of using 2 mm actuators in the large wind tunnel, smaller 1 mm actuators were employed due to the smaller size of the wing model.

Figure 29 shows the vortex structure with a linear array of 1 mm actuators at $\theta=50^\circ$. Also shown in Fig. 29 is a picture of a single vortex without any actuator for comparison. Flow accelerates near the leading edge and separates due to adverse pressure gradient. From figure 29(a), one can see flow separate at about $\theta=60^\circ$. If a linear array of actuators is employed at $\theta=50^\circ$, we can clearly see how the vortex structure has been distorted by the presence of the micro-actuators. First, it was found that the core of the vortex has indeed been moved outboard. This result agrees with surface pressure measurements. It was also observed that the direction of the shear layer separating from the leading edge had been altered. Since the location of the micro-actuators is ahead of the separation point, the flow could separate further upstream due to the higher adverse pressure-gradient caused by the presence of the micro-actuator. The separated shear layer follows the direction of the flap and moves further away from the wing surface. A positive rolling moment is generated by these two asymmetric vortices.

Figure 30 is the flow visualization picture of the vortex with a linear array of 1 mm actuators at $\theta=80^\circ$. Similar to the data from surface pressure measurements, it was found that the core of the vortex had shifted inboard. It was also noticed that the direction of the shear layer separating from the leading edge becomes closer to the surface. The possible mechanism is as follows: The flap actuator moves away from the surface and reduces the local curvature, such that the adverse pressure gradient is reduced. As a result, the flow follows the surface and the separation is delayed. Thus, the separated shear layer takes off at a shallow angle and the vortex moves in board. A negative rolling moment is then generated by these asymmetric vortices.

CONCLUDING REMARKS

MEMS technology can be used to batch fabricate sensors and actuators in extremely small sizes. These transducers can be one or more orders of magnitude smaller than the ones made by traditional techniques so that the temporal and spatial resolutions can be greatly improved. Another property of the micromachined sensors and actuators is that they can be monolithically integrated with microelectronics such that closed-loop systems for flow control can be established. In this work, an example of using a large-scale MEMS system has been shown to achieve distributed flow control.

The objective of this task was to demonstrate the feasibility of using micro sensors and actuators to control a macro aerodynamic device. We demonstrate that the motion of a delta-wing aircraft can be controlled by manipulating the separation around the leading edges of the delta wing. A pair of symmetric vortices wrapping around the leading edge characterizes the flow over a delta wing. At high angles of attack, these vortices contribute a significant portion to the total lift. Hence, if the symmetry of these vortices can be broken by micro-actuators, it is possible to generate a rolling moment, or pitching and yawing moments by proper spatial actuation. The key point for this kind of flow control is matching of length scale. If the size of the micro-actuator matches the thickness of the thin boundary layer near the leading edges of the delta wing, it is possible to use these small actuators to perturb the flow and break the symmetry of the two leading-edge separation vortices. This matching provides a coupling between the micro-actuator and the flow instability, which serves as an effective flow amplifier of the artificial disturbances.

A flexible skin containing a large number of densely arrayed shear-stress sensors was used to provide instantaneous detection of the flow separation line. This was the first time that successful measurements of the shear stress distribution along rounded leading edges of a delta wing were documented. It was found that the flow could separate at different locations due to the local curvature, Reynolds number, and pressure gradient. The separation line is a curved line along the leading edges. In order to control the curved separation line efficiently, it is necessary to have a distributed flow control system. This is one of the reasons that MEMS technology is useful in this work since the motion of individual micromachined actuators can be controlled.

After the detection of the instantaneous separation line, micromachined actuators were employed at the appropriate locations to manipulate the flow inside the thin boundary layer, resulting in significant increases in

rolling, pitching, and yawing moments. The maximum pitching and rolling moment coefficients generated by micro-actuators could be as large as 0.03 and 0.012, respectively.

Aerodynamic tests, including surface pressure measurements and flow visualization, were conducted to investigate the physical mechanisms for vortex control. By interpreting data from these experiments, the physical mechanisms for torque generation have been confirmed. It was found that the positions of vortices are shifted due to the presence of micro-actuators. It was also observed that the micro-actuators would alter the deflection angle of shear layer. As a result, a large rolling moment could then be obtained.

Instead of using large flaps to change the camber of the wing as a means of flow control, micromachined sensors and actuators were used to control leading-edge vortices on the suction side of the delta wing, generating large torques suitable for aircraft control. The delta wing experiments have demonstrated that micro-actuators can be used to influence the global aerodynamics of the aircraft, and generate enough torque for aircraft control.

Acknowledgment

This work is supported by the DARPA ETO.

References

- ¹Petersen, K. E., "Silicon as a Mechanical Material," Proc. IEEE, Vol. 70 (5), pp. 420-456, 1982.
- ²Madou, M., "Fundamentals of Microfabrication", CRC Press, New York, 1997.
- ³Ho, C.M. and Tai, Y.C., "Micro -Electro-Mechanical-Systems and Fluid Flows," Annual Review of Fluid Mechanics, Vol. 30, pp. 579-612, 1998.
- ⁴Lee, G. B., Ho, C. M., Jiang, F., Liu, C., Tsao, T., and Tai, Y. C., "Distributed Flow Control by MEMS", ASME 1996 International Mechanical Engineering Congress and Exposition, Atlanta, Georgia, USA, Nov. 17-22, 1996.
- ⁵Ho, C.M. and Tai Y.C., "MEMS and its applications for Flow Control". Journal of Fluid Engineering, Vol. 118, pp. 437-447, 1996.

- ⁶Tung, S., Hong, W., Ho, C. M., Liu C., and Tai, Y.C., "Control of Streamwise Vortices in 2-D Channel Flows, " Proceedings, The 6th Congress of Asian Fluid Mechanics, Singapore, May, 1995.
- ⁷Liu, J., Tai, Y.C., Pong, K., and Ho, C. M., "MEMS for Pressure Distribution Studies of Gaseous Flows in Microchannels," Proceedings, IEEE Micro Electro Mechanical Systems, pp. 209-215, Amsterdam, the Netherlands, Jan. 29, 1995.
- ⁸Bradley R. G. and Wray W. O., "A Conceptual Study of Leading -Edge-Vortex Enhancement by Blowing", Journal Aircraft, vol.11, No. 1, 1974, pp. 33-38.
- ⁹Wood, N. J. and Roberts, L., "The Control of Vortical Lift on Delta Wings by Tangential Leading Edge Blowing", AIAA paper No. 87-0158.
- ¹⁰Hummel, D., "Zur Umströmung sharfkantiger schlanker Deltaflügel bei grossen Anstellwinkeln", Z. Flugwiss., Vol. 15, No. 10, 1967, pp. 376-385.
- ¹¹Wahls R. A., Vess R. J. and Moskovitz C. A., "Experimental Investigation of Apex Fence Flaps on Delta Wings", Journal of Aircraft, vol. 23, No. 10, 1986, pp. 789-797
- ¹²Marchman III J. F. "Aerodynamics of Inverted Leading-Edge Flaps on Delta Wings", Journal of Aircraft, vol. 18, No. 12, 1981, pp.1051-1056
- ¹³Marchman III J. F., "Effect of heating on Leading Edge Vortices in Subsonic Flow", Journal of Aircraft, vol. 12, No. 2, 1975, pp. 121-123.
- ¹⁴Liu, C., Tai, Y.C. Huang, J. and Ho, C. M., 1994, "Surface-Micromachined Thermal Shear Stress Sensor," Application of Microfabrication to Fluid Mechanics, FED-Vol. 197, pp. 9-16, ASME.
- ¹⁵Maltby, R. L., "The Development of the Slender Delta Concept," Aircraft Engineering, March 1968.
- ¹⁶Lambourne N. C. and Bryer D.W., "The Bursting of Leading -Edge Vortices-Some Observations and Discussion of the Phenomenon," Aero. Res. Council, Reports and Memoranda, No. 3282, 1961, pp. 1-37.
- ¹⁷Polhamus E. C., "A Concept of the Vortex Lift of Sharp-edge Delta Wings Based on a Leading-edge-suction Analogy," NASA TN D-3767, 1966.
- ¹⁸Lee, G. B., Jiang, F., Tsao, T., Tai, Y. C., Ho, C. M., "Macro Aerodynamics Devices Controlled by Micro Systems", 1997 IEEE Aerospace Conference, Snowmass, Colorado, Feb. 1-8, 1997.

- ¹⁹Ho, C. M., Tung, S., Lee, G. B., " MEMS- A Technology for Advancements in Aerospace Engineering", AIAA 35th Aerospace Sciences Meeting & Exhibit, AIAA 97-0545, Jan. 6-10, 1997, Reno, NV.
- ²⁰Liu C., Tsao T., Tai Y. C. and Ho C. M., 1994, "Surface Micromachined Magnetic Actuators," Proceed. IEEE International Workshop on MEMS, MEMS'94, Oiso Japan.
- ²¹Grosjean, C., Lee, G. B., Hong, W., Tai, Y. C., Ho, C. M., " Micro Balloon Actuators For Aerodynamic Control", IEEE Micro Electro Mechanical Systems, German, January 1998.
- ²²Panton, R. L., "Incompressible Flow," John Wiley & Sons, Inc, 1984.
- ²³Jiang, F., Tai, Y. C., Walsh, K., Tsao, T., Lee, G. B., Ho, C. M., " A Flexible MEMS Technology and Its First Application to Shear Stress Sensor Skin", IEEE MEMS-97 Workshop, Japan, January, 1997.
- ²⁴White, F. M., Fluid Mechanics, 3rd ed., McGraw Hill, New York, 1994, pp.413 - 422.
- ²⁵Bellhouse, B. J. and Schultz D. L., " Determination of mean and dynamic skin friction, separation and transition in low-speed flow with a thin-film heated element ", Journal of Fluid Mechanics, vol. 24, part 2, pp. 379 - 400, 1966.
- ²⁶Gwo-Bin Lee, " Control of a Delta-Wing Aircraft by Using Micromachined Sensors and Actuators", Ph.D. thesis, UCLA, 1998.
- ²⁷Anderson, J. D., "Introduction to Flight," McGraw-Hill, 1985.

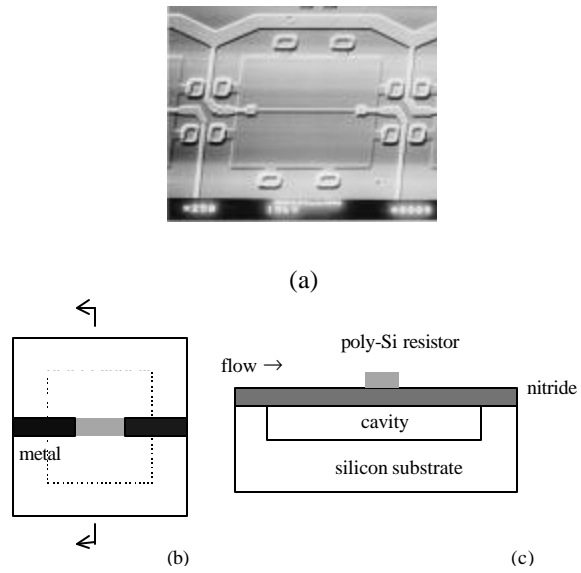


Fig. 1 (a) SEM picture, (b) top view, and (c) cross-sectional views of the micro shear-stress sensor.

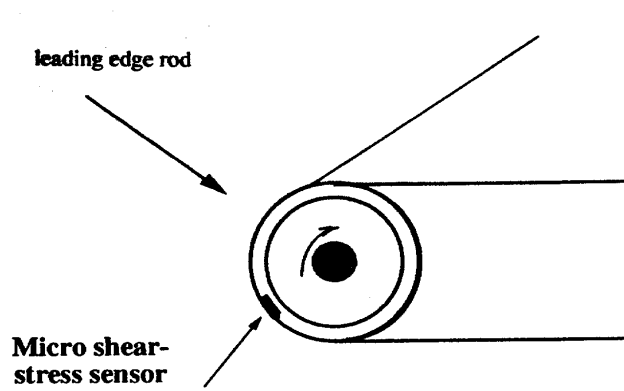


Fig. 2 Micro shear stress sensor located on a rod at the leading edge of a delta wing

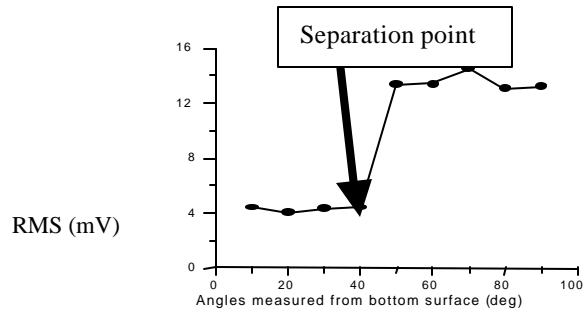


Fig. 3 RMS signal from a micro shear stress sensor for different locations

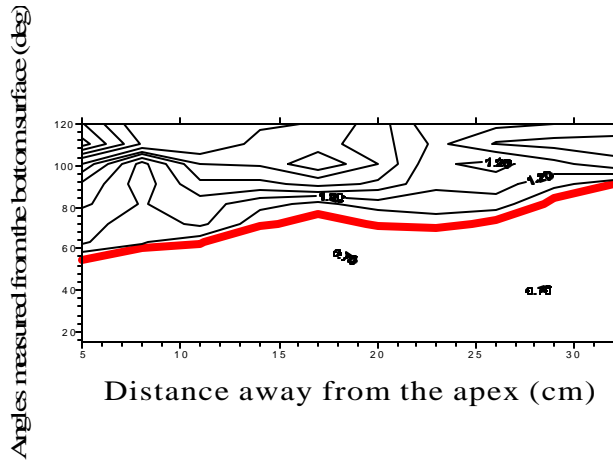


Fig. 4 Separation line for the case of 25 m/s, AOA=30°

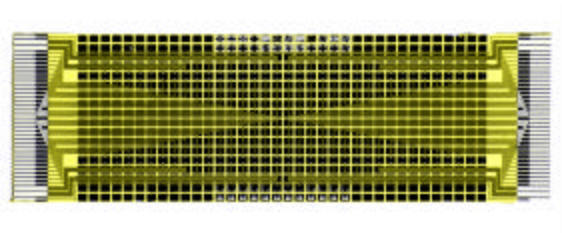


Fig. 5 Flexible skin with shear stress sensor array (Jiang et al. 1997)

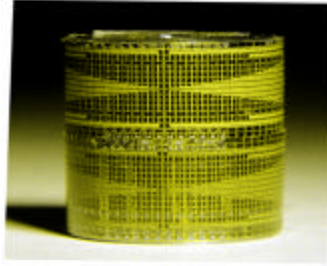


Fig. 6 Flexible skin on a circular cylinder (Jiang et al. 1997)

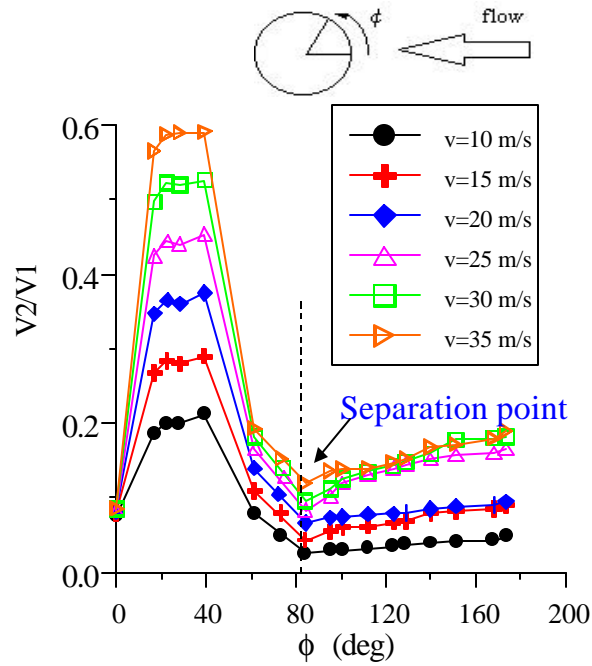


Fig. 7 DC output from flexible skin at different velocities

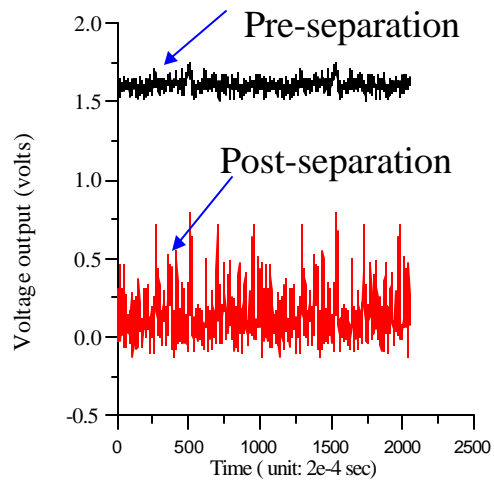


Fig. 8 Signal from flexible skin before and after flow separation

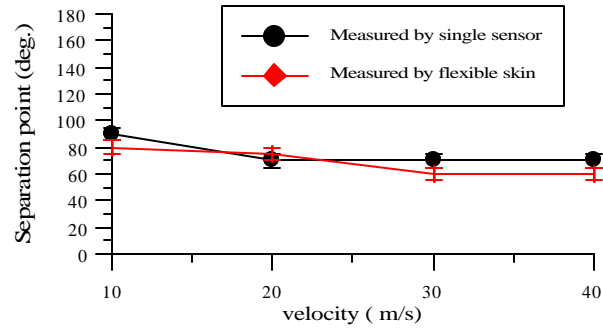


Fig. 9 Comparison of the results between flexible skin and a single sensor

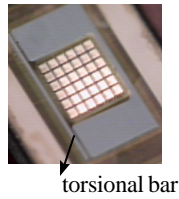
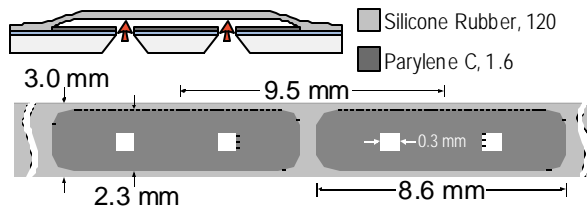


Fig. 10 Micro flap actuator



11(a)



11(b)

Fig. 11 (a) Schematic of micro balloon actuators, (b) Micro balloon actuator (Grosjean, 1998)

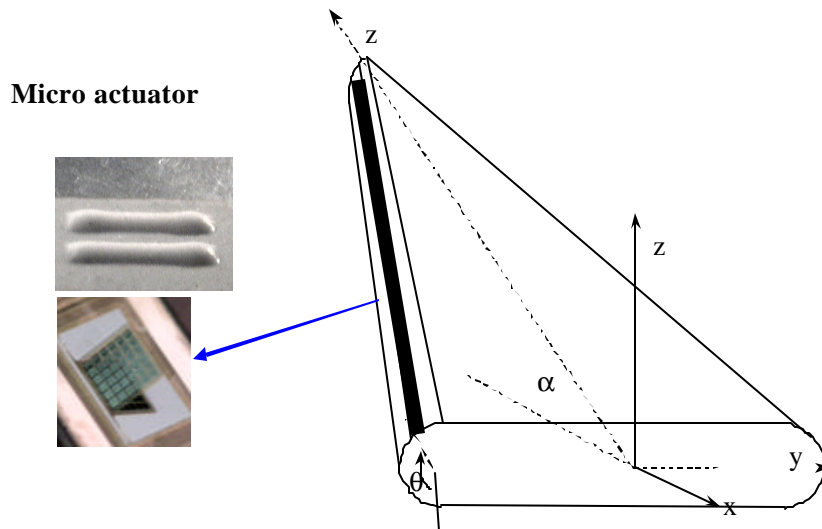


Fig. 12 A linear array of actuators on one of leading edges

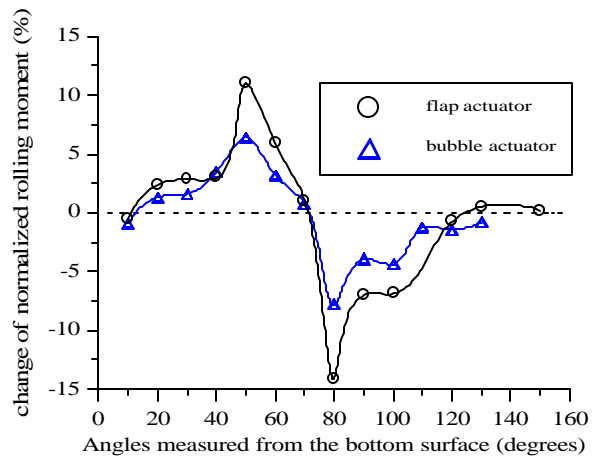
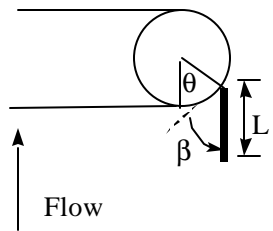


Fig. 13 Normalized rolling moment vs. 1 mm actuation locations at AOA=25°



θ : angle measured from bottom surface
 β : deflection angle
 L : size of actuators

Fig. 14 Schematic of deflection angle for micro actuators

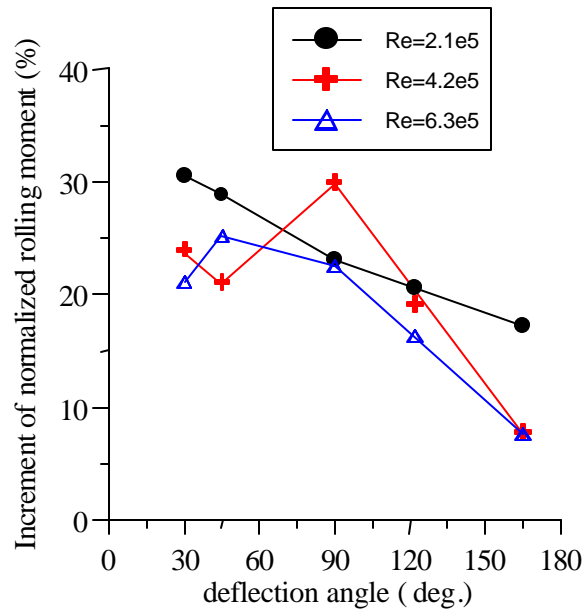


Fig. 15 Normalized rolling moment vs. deflection angle

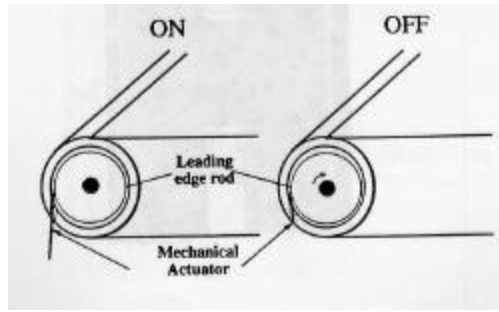


Fig. 16 Mechanical actuators

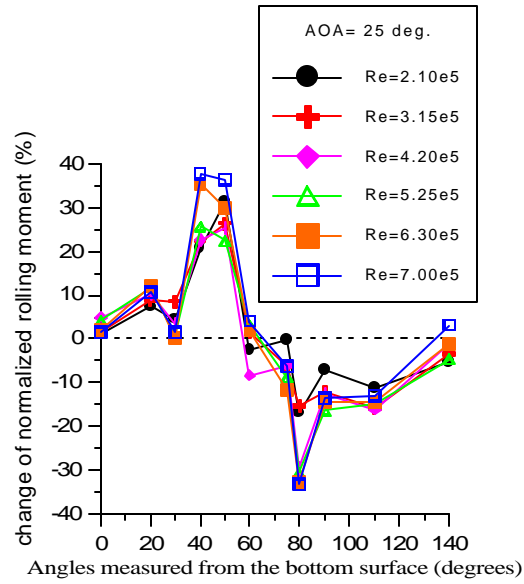


Fig. 17 Normalized rolling moment vs. 2 mm actuation locations at AOA=25°

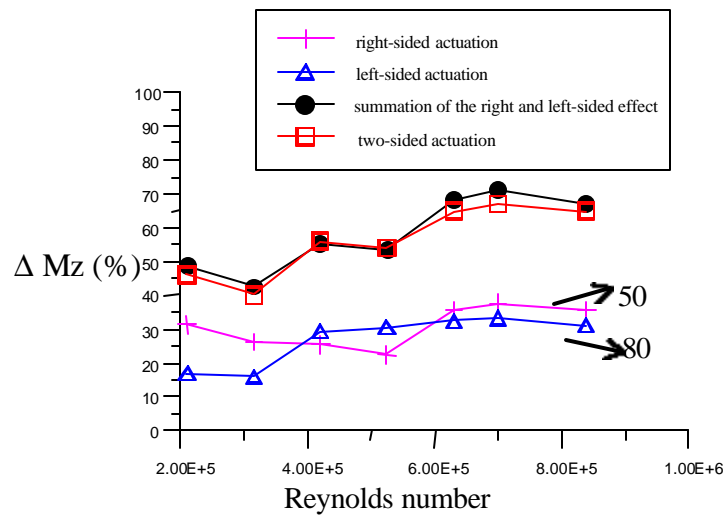


Fig. 18 Two-sided actuation effect at AOA=25°, 2 mm actuators

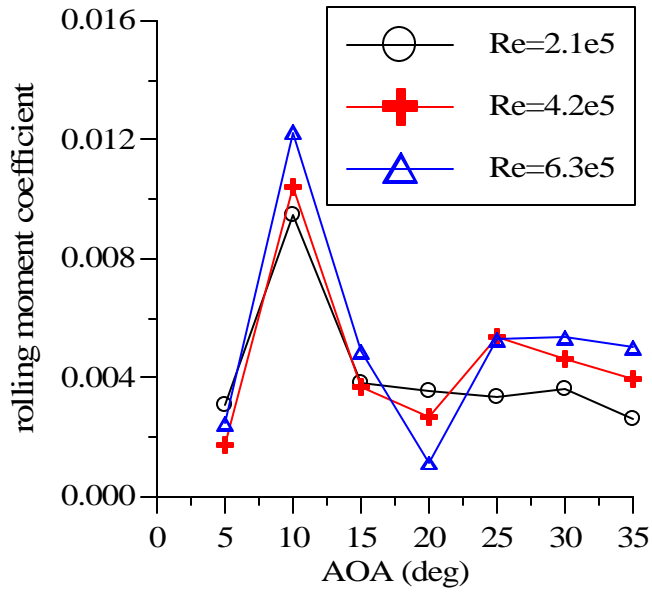


Fig. 19 Rolling moment coefficient vs. AOA

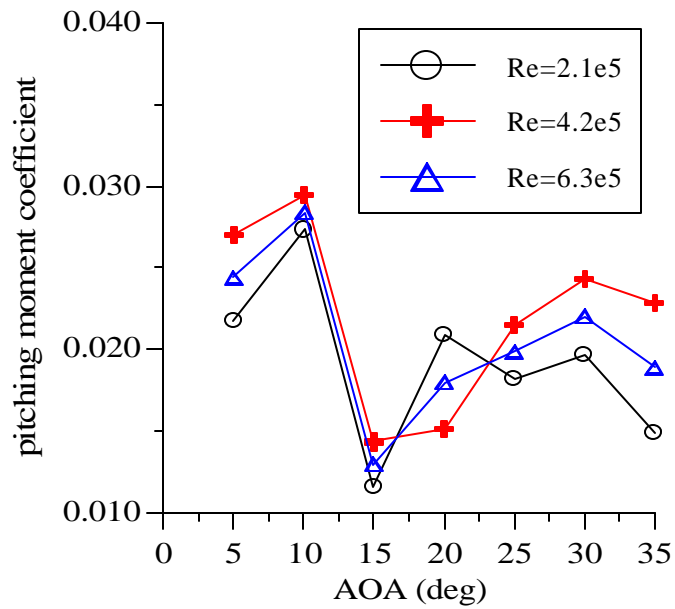


Fig. 20 Pitching moment coefficients vs. AOA

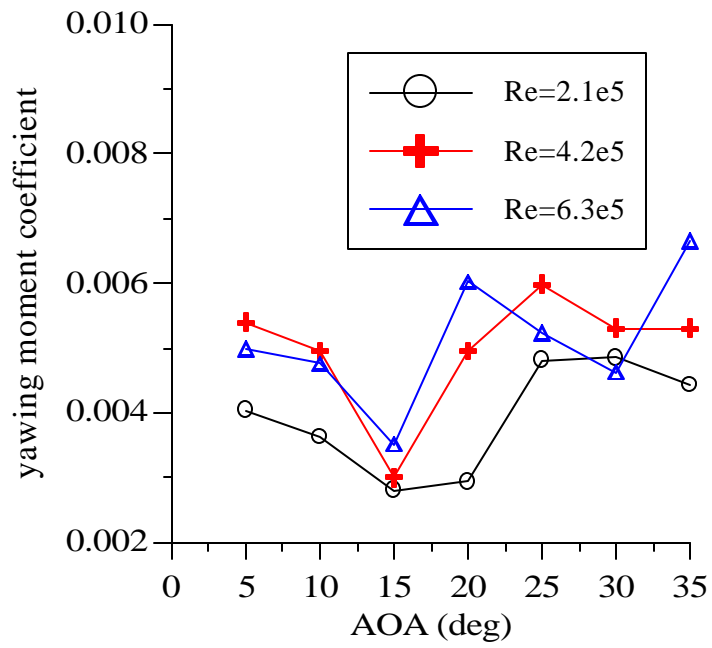


Fig. 21 Yawing moment coefficient vs. AOA

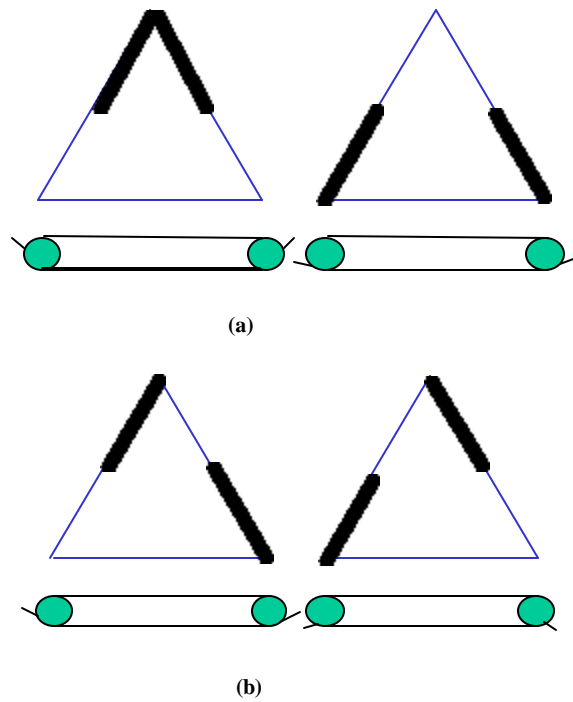


Fig. 22 (a) Pitching, (b) Yawing Moment Control by H-A-T Actuators

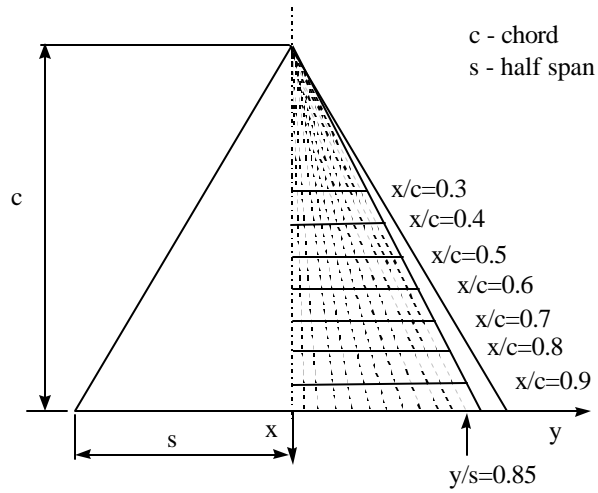


Fig. 23 Schematic setup for surface pressure measurement for a delta wing

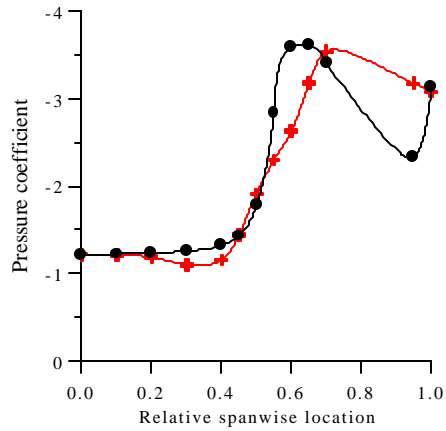


Fig. 24 Pressure distribution at AOA=25°, q=50°

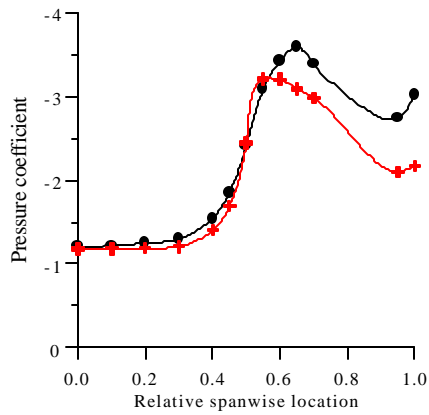


Fig. 25 Pressure distribution at AOA=25°, q=80°

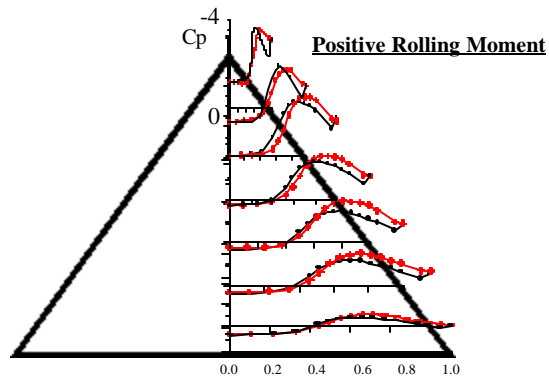


Fig. 26 Pressure coefficient variation along spanwise direction at AOA=25°, 2 mm actuators at $q=50^\circ$

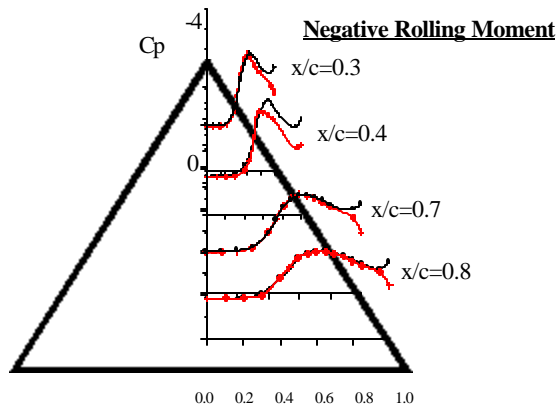


Fig. 27 Pressure coefficient variation along spanwise direction at AOA=25°, 2 mm actuators at $q=80^\circ$

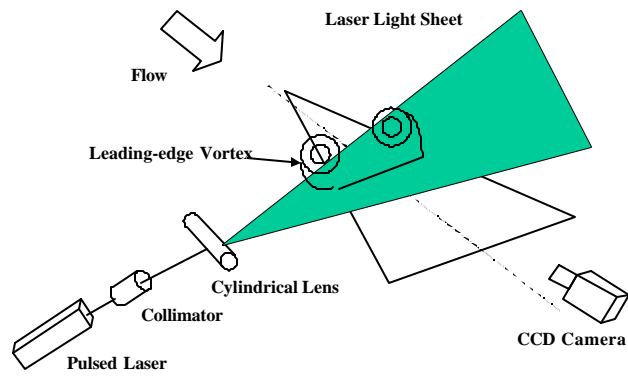


Fig. 28 Experimental setup for flow visualization

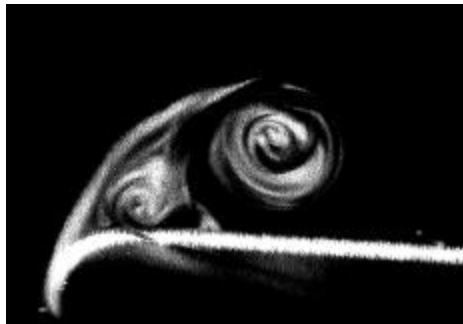


Fig. 29 (a) vortical structure before actuation

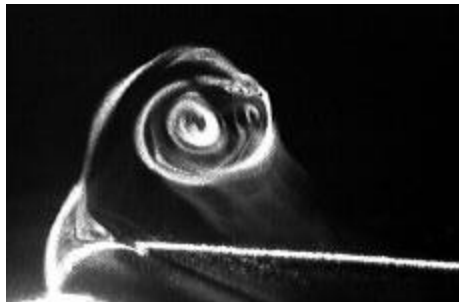


Fig. 29 (b) vortical structure after actuation at $q=50^\circ$

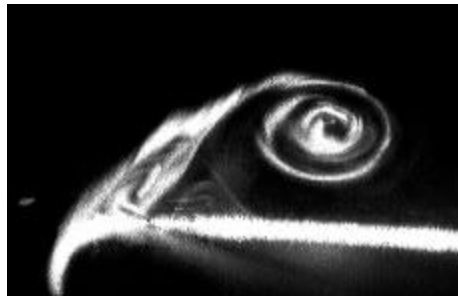


Fig. 30 Vortical structure after actuation at $q=80^\circ$